

Fermi surface of $\text{Cr}_{1-x}\text{V}_x$ across the quantum critical point

J.F. DiTusa,^{1,*} R. G. Goodrich,² N. Harrison,³ and E. S. Choi⁴

¹*Department of Physics and Astronomy, Louisiana State University, Baton Rouge, Louisiana 70803, USA*

²*Department of Physics, George Washington University, Washington, DC 20052, USA*

³*National High Magnetic Field Laboratory, Los Alamos National Laboratory,
MS E536, Los Alamos, New Mexico 87545, USA*

⁴*National High Magnetic Field Laboratory, Florida State University, Tallahassee, Florida 32310, USA*

(Dated: May 24, 2022)

We have measured de Haas-van Alphen oscillations of $\text{Cr}_{1-x}\text{V}_x$, $0 \leq x \leq 0.05$, at high fields for samples on both sides of the quantum critical point at $x_c = 0.035$. For all samples we observe only those oscillations associated with a single small hole band with magnetic breakdown orbits of the reconstructed Fermi surface evident for $x < x_c$. The absence of oscillations from Fermi surface sheets most responsible for the spin density wave (SDW) in Cr for $x > x_c$ is further evidence for strong fluctuation scattering of these charge carriers well into the paramagnetic regime. We find no significant mass enhancement of the carriers in the single observed band at any x . An anomalous field dependence of the dHvA signal for our $x = 0.035$ crystal at particular orientations of the magnetic field is identified as due to magnetic breakdown that we speculate results from a field induced SDW transition at high fields.

PACS numbers: 71.18.+y, 75.30.Fv, 71.27.+a, 75.40.Cx

INTRODUCTION

Chromium has fascinated condensed matter physicists since it was demonstrated to be antiferromagnetic, AFM, by Shull and Wilkinson[1] in 1953. The understanding of the spin density wave, SDW, ground state and its ramifications on the physical properties of this elemental metal was largely worked out over 30 years ago[2, 3]. However, more recently it was realized that the continuous suppression of the Néel temperature, T_N , to zero by the substitution of small amounts of V, Nb, or Ta, or by application of pressure made Cr an ideal simple material to explore the consequences of a quantum criticality[4, 5]. The results of investigations into this transition have been used to compare to more complicated systems where quantum critical points (QCP) are thought to dominate the physical properties over wide ranges of composition, temperature, pressure, and magnetic field. The association of superconductivity with QCPs has also fueled the interest in exploring such transitions. One well established method for accessing the Fermi surfaces, FS, of metals is the de Haas van Alphen, dHvA, effect[6] which is increasingly being employed to explore FS changes in materials near QCPs[7–12]. Here we measure the dHvA oscillations in $\text{Cr}_{1-x}\text{V}_x$ as x is varied through the critical concentration at $x = 0.035$ [2–5]. Our data near the simplest of QCPs should serve as a point of reference for the more complex quantum critical systems and may have consequences for their interpretation. Our experiments make use of very large magnetic fields that were not available to the earlier explorations[13–16] to extend the dHvA measurements through x_c where the doping induced disorder makes small cyclotron orbits a requirement for observation.

The incommensurate SDW state in Cr differs from classical AFMs as magnetic moments at the cube corners of the body centered cubic (bcc) structure are antiparallel, but not quite equal to the magnetic moments on the body-center. Their magnitude is modulated in a sinusoidal manner with a wavevector Q_{SDW} which lies along a [100] crystal axis. In pure Cr $Q_{SDW} = 0.953a^*$ at liquid helium temperature and is accompanied by a charge density wave modulation at $2Q_{SDW}$ [17]. Band structure calculations of the Fermi surface of paramagnetic (PM) bcc Cr is very similar to that of Mo and W, the other elements of column VIB of the periodic table[18–20]. These FSs are typically described as consisting of an electron jack centered at Γ , a hole octahedron centered on the H-points $[\pi/a, 0, 0]$, hole ellipsoids centered at the N-points $[\pi/2a, \pi/2a, 0]$, and small electron lenses along the Γ -H line of the conventionally labeled Brillouin zone. In Cr extensive nesting between the electron jack and the hole octahedron is responsible for the transition to the SDW state as Q_{SDW} connects these two parts of the FS so that they are gapped below $T_N = 313$ K. As a result only smaller sheets of the Fermi surface are expected to survive in the SDW phase in agreement with Hall effect experiments that reveal a substantial decrease in itinerant carriers below T_N [4, 5, 21]. V substitution reduces the electron density so that electron-like regions of the Fermi surface are expected to shrink in size while the hole-like regions expand. The result is a decreased area on the electron jack and hole octahedron which remain parallel and a decreased Q_{SDW} corresponding to an increased incommensurability with x . The area of parallel Fermi surfaces connected by Q_{SDW} appears to drop quickly for $x > 0.03$ [22] and the QCP is reached when the interaction area between the two FS sheets is reduced to the point where AFM cannot be sustained.

The periodicity caused by the condensation into the SDW phase also has dramatic consequences for the other FS sheets as the PM FS is remapped by translation through $\pm nQ_{SDW}$, where n is an integer[18, 19]. For the pockets of holes at the N-points this results in extensively overlapping hole ellipsoids (demonstrated schematically in Fig. 3 below) and, thus, open orbits along the direction of Q_{SDW} that have been detected in magnetoresistance and Hall effect measurements in single domain samples[23, 24]. Previous dHvA measurements in Cr revealed a large number of small k -space area orbits caused by the magnetic breakdown between these intersecting hole surfaces. No other pieces of the Fermi surface have been successfully observed with this method in contrast to dHvA experiments performed on Mo[25] and W[26] where the larger FS sheets are apparent. Angle-resolved photoemission (ARPES) measurements of the electronic structure of $\text{Cr}_{1-x}\text{V}_x$ thin films[27, 28] observe all of the dispersing bands and indicate a complete gapping of the electron jack and hole octahedron in the SDW phase. Measurements of the FS of $\text{Cr}_{1-x}\text{V}_x$ for $0 \leq x \leq 1$ via two dimensional angular correlation of electron-positron annihilation radiation techniques (2D-ACAR) observed each of the FS sheets and carefully followed the evolution of the pocket of holes at the N-points for comparison to measurements of the giant magnetoresistance effect in multilayers with Cr spacers[29]. dHvA measurements in dilute V substituted samples ($x < 0.01$) observed small changes consistent with a reduction of Q_{SDW} with x without a measurable change to the cross sectional area of the N-pockets of the Fermi surface[30]. In addition dHvA measurements on Mn doped Cr, where the SDW phase becomes commensurate for concentrations of 1% or larger[31], reveal a smaller number of oscillation frequencies corresponding to a much simpler Fermi surface.

Here we find that V substitution leads to changes in the observed frequencies in the dHvA spectra consistent with an increased area of the hole ellipsoid at the N-point along with a decreased Q_{SDW} for $x < x_c$. For $x \geq x_c$ we observe a much simpler dHvA spectra as only signals associated with a *single* ellipsoid are apparent. We interpret the absence of observed frequencies associated with the larger FS sheets for PM Cr as indicating that the scattering of these carriers due to the SDW fluctuations remains strong, even for $x = 0.05$. This is consistent with previous transport measurements[4, 5] showing little change in the low temperature carrier conductivity. In addition, for $x = 0.035$ we observe changes to the spectra that indicate the existence of magnetic breakdown orbits for fields larger than ~ 20 T. We speculate that these orbits may be indicating a return to the SDW state due to the changes in the FS geometry with field, a field induced SDW transition for samples just on the PM side of the QCP.

EXPERIMENTAL DETAILS

Single crystals of Cr, $\text{Cr}_{0.98}\text{V}_{0.02}$, $\text{Cr}_{0.965}\text{V}_{0.035}$, and $\text{Cr}_{0.95}\text{V}_{0.05}$ were grown at Ames laboratory from high purity starting materials by arc melting, arc zone refinement, and heat treatment at 1600°C for 72 hours. These crystals were oriented by back reflection Laue and were spark cut so that faces were perpendicular to $[100]$ directions. The resulting single crystals had approximate dimensions of $0.25 \text{ mm} \times 0.25 \text{ mm} \times 0.1 \text{ mm}$ thick. Resistivity measurements of our nominally pure and $x = 0.02$ crystals displayed anomalies associated with T_N within 1 K of those found in previous measurements[32] of samples with the same stoichiometry. No anomaly was found for our $x = 0.035$ and 0.05 samples indicating, as expected, that $x > x_c$. Some of the dHvA measurements were made between 0 and 55 T at the pulsed field facility of the National High Magnetic Field Laboratory (NHMFL) located at the Los Alamos National Laboratory. Angular dependent measurements were made between 0 and 33 T at the NHMFL branch located in Tallahassee, FL using a cantilever to measure the torque on the sample as the field was changed. Details of both of these measurement techniques have previously been reported[33].

DE HAAS-VAN ALPHEN SPECTRA

The oscillatory magnetic susceptibility that we observe in our pulsed field dHvA measurements is demonstrated in Fig. 1a during both the injection of current into the magnet windings and the somewhat slower decay of the field for a nominally pure Cr crystal. The Fourier transforms of these signals for 2 Cr crystals as well as from a $\text{Cr}_{0.98}\text{V}_{0.02}$ and a $\text{Cr}_{0.965}\text{V}_{0.035}$ crystal is displayed in Fig. 2. For our nominally pure Cr crystals, we observe a number of narrow, well defined, dHvA frequencies between 100 and 2400 T that agree well with previous measurements[13–16] represented in Fig. 2a by the dashed lines. There are several orbits, labeled χ , ρ , and μ that were seen in the previous dHvA measurements in the orientation where magnetic field is parallel to Q_{SDW} that do not appear in our data. Since our crystals were cooled through T_N in zero magnetic field, we expect our samples to have multiple AFM domains with Q_{SDW} oriented along each of the equivalent $[100]$ crystal axes. The absence of signals for the frequencies associated with Q_{SDW} parallel to H indicates that our experiments are somehow insensitive to these orbits. We also find a number of smaller amplitude signals at frequencies above 2.5 kT that we identify as either simple harmonics, or reunion orbits, of the signals displayed in Fig. 2. In addition, we observe a large number of small amplitude signals at $f < 1000$ T that grow as the temperature is reduced below 1.5 K which are not yet identified. The large number of frequencies that appear in the dHvA spectra of Cr,

described previously as 'pseudo-harmonic', are due to the reconstruction of the FS of paramagnetic Cr by the periodicity of the incommensurate SDW state. The remapping of the FS allows a number of magnetic breakdown orbits which we identify in Fig. 2a and in Fig. 3 where we reproduce a schematic demonstrating several of the cyclotron orbits of the hole surface at N[13, 14]. First, second, and third order magnetic breakdown orbits are allowed, as well as reunion orbits. Despite the large increase in magnetic field range afforded by the pulsed field magnets, no signal from either the 'electron jack' or the 'hole octahedron' portions of the FS could be identified.

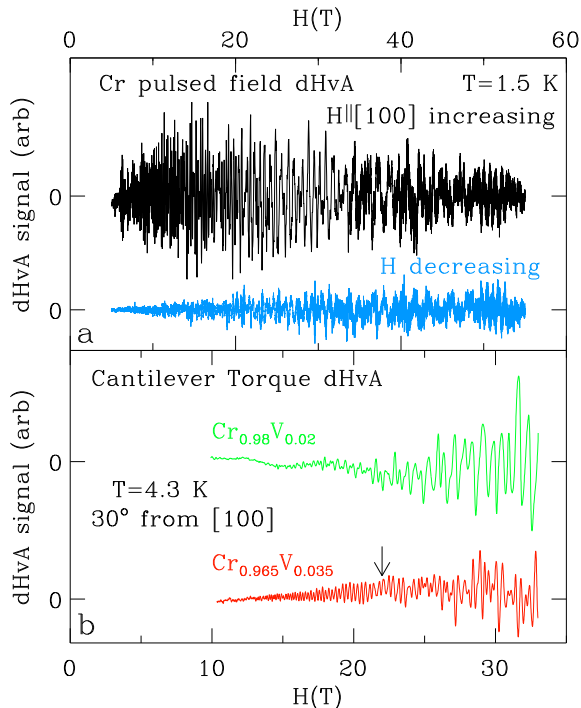


FIG. 1: (color online) de Haas-van Alphen oscillations from the pulsed field and torque cantilever measurements. a) Pickup coil signal for the pulsed field measurement of a nominally pure Cr crystal oriented with the magnetic field, H , parallel to the crystal $[100]$ direction. The data were taken at 1.5 K and the signal is shown for both increasing and decreasing magnetic fields. b) Torque signal from the cantilever measurements of the dHvA oscillations for a $\text{Cr}_{0.98}\text{V}_{0.02}$ and a $\text{Cr}_{0.965}\text{V}_{0.035}$ single crystal. Data taken at 4.3 K with the magnetic field oriented 30° from the $[100]$ crystal axis. Arrow indicates the field (22 T) where magnetic breakdown is evident in the $x = 0.035$ sample at this orientation, see text.

Although the large field used did not result in the detection of new oscillation frequencies related to the sheets of FS most closely associated with the SDW state, it was sufficient to access signals from the same FS pockets in our V-substituted crystals. This is apparent in Fig. 2c and d for our $x = 0.02$ and $x = 0.035$ crystals where distinct frequencies of oscillation are apparent below 14 K. The low frequency spectra, $f < 1$ kT, of our

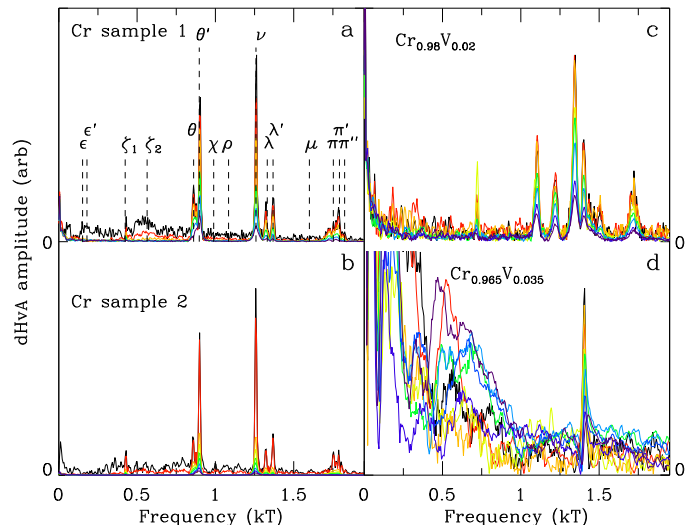


FIG. 2: Fourier transforms of the de Haas-van Alphen oscillations from the pulsed field measurements. a) and b) Fourier transforms (FFT) of de Haas-van Alphen, dHvA, signal for two Cr crystals at temperatures, T , of 1.45 (black), 2.5 (red), 4.2 (orange), 8.0 (green), 12.0 (blue), and 16 K (violet) for (a) and 0.45 (black), 1.45 (red), 4.2 (orange), 6.0 (yellow), 8.0 (yellow-green), 10.0 (green), 13.0 (blue), 16.0 (purple), and 20 K (violet) in (b). c) FFT of dHvA signal for $\text{Cr}_{0.98}\text{V}_{0.02}$ at T s of 0.85 (black), 1.5 (red), 2.4 (orange), 4.2 (yellow), 6.0 (green), 8.0 (blue), 12.0 (purple), and 14.0 K (violet). d) FFT of the dHvA signal for $\text{Cr}_{0.965}\text{V}_{0.035}$ at T s of 0.50 (black), 1.5 (red), 2.0 (orange), 4.2 (yellow), 6.0 (green), 8.0 (blue), 10.0 (dark blue), 12.0 (purple), and 14.0 K (violet). All data taken with the magnetic field, H , parallel to a $[100]$ crystal axis with FFTs calculated for fields between 15 and 55 T. The dashed lines in (a) indicate the dHvA frequencies reported in Ref. [15, 16] and we employ the labels adopted previously for these frequencies.

$x = 0.035$ crystal is dominated by, what appear to be, noise that grows with magnetic field. For $x = 0.02$ the spectra contains a large number of peaks with f similar to that seen in pure Cr, although the peaks appear to be broader despite the identical field range used to compute the FFTs. The most obvious differences with pure Cr are the changes in the relative amplitudes of the peaks and the shifting of several of the peaks to higher frequency. These changes are expected since, naively, V-substitution is known to reduce the electron density and, consequently, increase the size of the hole pocket thus reducing the SDW wave vector. The result is that the amplitude of the dHvA frequency associated with the unreconstructed FS, labeled λ in Fig. 2a, grows relative to the amplitude of the other magnetic breakdown orbits and its frequency increases by 30 ± 5 T per 1% V substitution. There are much more dramatic changes evident in the $x = 0.035$ dHvA spectra shown in Fig. 2d. Here we observe only a single frequency at 1.4 kT which is slightly larger than that identified as the λ orbit in frames a and b of the figure. Thus, as we approach V

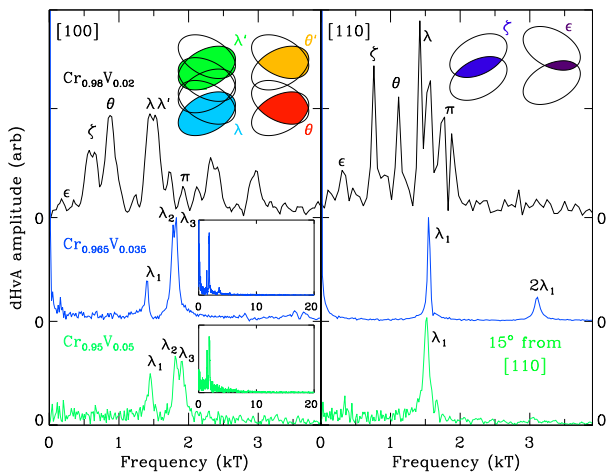


FIG. 3: Fourier transforms of the de Haas-van Alphen oscillations from torque cantilever measurements. FFT of the dHvA signal for fields parallel to a [100] crystal axis (left side) and parallel to a [110] crystal axis (right side) for $\text{Cr}_{0.98}\text{V}_{0.02}$ (black), $\text{Cr}_{0.965}\text{V}_{0.035}$ (blue), and $\text{Cr}_{0.95}\text{V}_{0.05}$ (green) (at 15° from the [110] direction) crystals taken over a field interval of between 10 and 33 T. All data at 4.2 K except $x = 0.05$ data with field parallel to [100] which was at 0.7 K. Insets show the data over an extended frequency range displaying the absence of higher frequency oscillations that may be related to the larger FS sheets of paramagnetic Cr. Drawings at the top of figure are of a schematic representation (not to scale) in an extended zone scheme of the magnetic breakdown orbits that occur between intersecting hole ellipsoids formed by the remapping of the paramagnetic Fermi surface by translation by multiples of the spin density wave vector [13, 14].

concentrations where the SDW phase is suppressed, we no longer observe the large number dHvA signals associated with the remapping of the FS due to the formation of the SDW state. This observation further supports the picture developed from the earlier measurements of the dHvA in pure Cr, that of pseudoharmonic dHvA signals resulting from the remapping of the Fermi surface.

Our torque cantilever measurements of the dHvA oscillations, demonstrated in Fig. 1b, yield similar spectra as can be seen in Fig. 3 where we display our data for $x = 0.02, 0.035,$ and 0.05 crystals for two field orientations. Data taken in this manner allows a much cleaner exploration for low frequencies where our pulsed field data suffered from higher noise levels. The crystals were carefully rotated in field by increments of 5 or 10° in the [001] plane for all three samples, and in the [011] plane for the $x = 0.035$ sample, to probe the variation of the Fermi surface. The same general trends with x that we observed in our pulsed field data are also apparent in these data, the most important being the absence of pseudoharmonic magnetic breakdown orbits for our $x = 0.035$ and $x = 0.05$ samples. The variation of the 3

observed frequencies in the dHvA spectra, labeled $\lambda_1, \lambda_2,$ and λ_3 in Fig. 3, for our $x = 0.035$ and $x = 0.05$ samples with rotation of the crystal with respect to the magnetic field is displayed in Fig. 4. Both the rotation symmetry of these signals, as well as the ratio of these frequencies at high symmetry points are nearly identical to a set of dHvA frequencies measured in Mo [25]. These frequencies are identified as emanating from a single Fermi surface sheet, the small pocket of holes at the N-point of the Mo Brillouin zone. Therefore, we make the same identification for the dHvA frequencies we observe in $\text{Cr}_{1-x}\text{V}_x$ for $x > x_c$. We emphasize that we do not observe dHvA oscillations that can be associated with any other pieces of the FS in any of our samples, even in our $x = 0.05$ sample which is well beyond the critical concentration for the SDW ground state.

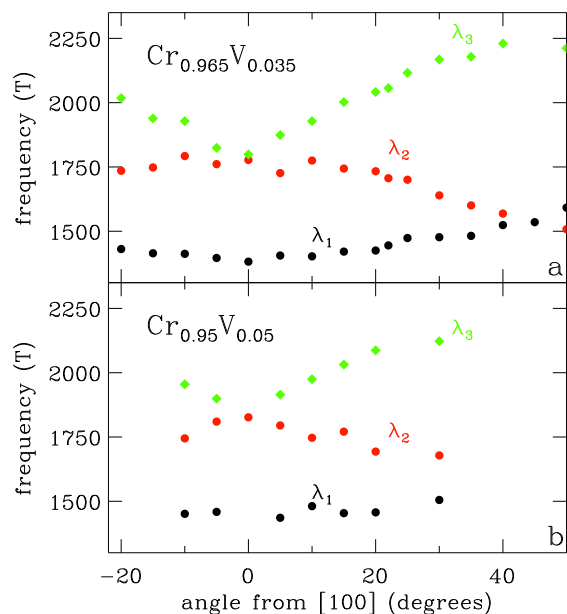


FIG. 4: (color online) Angle dependence of the de Haas-van Alphen frequencies. The variation of the three frequencies detected in the dHvA spectra with the angle between the crystal [100] axis and the magnetic field for rotations in the [001] plane for a) $\text{Cr}_{0.965}\text{V}_{0.035}$ and b) $\text{Cr}_{0.95}\text{V}_{0.05}$. The three frequency branches labeled $\lambda_1, \lambda_2,$ and λ_3 originate from the pocket of holes centered at the N-point of the Brillouin zone of paramagnetic Cr. A very similar set of frequencies is evident in the dHvA spectrum of Mo [25] along with a large number of other frequencies from the other Fermi surface sheets.

THE EFFECTIVE MASS AND SCATTERING RATES

Despite the changes to the spectra that we measure with x , the dHvA signals do not have strong temperature dependencies at any x , including our $x = 0.035$ sample which lies closest to x_c . In Fig. 5 the amplitude

of the observed dHvA frequency identified as λ (λ_1) in our pulsed field dHvA spectra is plotted for the nominally pure and V substituted samples as a function of T . It is clear from this figure that there is a very slow decay of the amplitude of the dHvA signals with T for all 4 samples. The lines in the data are fits of the standard Lifshitz-Kosevich formula[6] to the data and the carrier masses which result from these fits are plotted in the inset. We observe no significant mass enhancement near the QCP, or any other trends, for the FS sheets that we are able to probe in this experiment. This is in accord with previous determinations of the carrier masses from dHvA in pure Cr[13], as well as measurements of the linear coefficient of the specific heat in zero field[34] where an increase from 1.3 to 2 mJ/mole K² was found in going from $x = 0$ to $x = 0.05$, and estimates based upon magnetic neutron scattering[35] in V-doped samples. Our analysis of the amplitude reduction with temperature of the λ orbit, in both our pulsed field and torque cantilever measurements, reveal no significant change of carrier mass from 0.5 ± 0.1 times the bare electron mass of pure Cr[14].

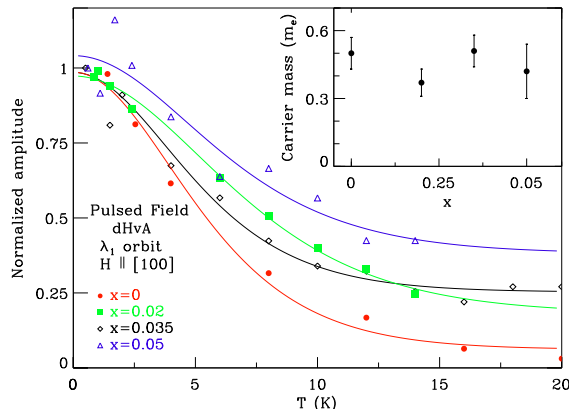


FIG. 5: (color online) Temperature dependence of a de Haas-Alphen frequency. The variation of the λ (λ_1) frequency with temperature for $\text{Cr}_{1-x}\text{V}_x$ as identified in the figure with the magnetic field, H oriented parallel to the [100] crystal axis. The lines represent fits of the Lifshitz-Kosevich formula[6] to the data to determine the cyclotron mass of the charge carriers. Inset: Charge carrier cyclotron mass as determined from the fits of the data in the main frame plotted vs. vanadium concentration, x . No measurable mass enhancement is observed near the critical concentration for spin density wave ground state at $x = x_c = 0.035$.

One of the features of the dHvA technique is that it allows the determination of scattering rates, τ^{-1} , for the charge carriers residing on different parts of the Fermi surface. This is done by measuring the amplitude of the λ orbit as a function of magnetic field to determine the Dingle temperature, $\Theta_D = \hbar/2\pi k_B \tau$, where k_B is Boltzmann's constant. The dHvA amplitude, A_p , for the p 'th harmonic of f can be expressed as a func-

tion of field as $A_p \propto TH^{-n} \exp(-pZ\Theta_D)/\sinh(p\alpha T/H)$, where $n = -1/2$ for torque cantilever measurements or $n = 5/2$ for the pulsed field measurements, $Z = \alpha/H$, and $\alpha = 2\pi^2 k_B m^* c/e\hbar$ [6]. In Fig. 6 we plot the amplitude of the λ orbit determined from the torque cantilever measurements for our $x = 0.035$ crystal at 4.2 K as a function of field for several orientations of the crystal. The typical form is apparent for orientations of the field at 20 and 63° from the [100] crystal axis, whereas at some angles significant deviations from the standard behavior is observed. The most obvious of these deviations occurs at an angle of 30° for fields above ~ 22 T corresponding to the raw dHvA data in Fig.1b where we plot an arrow to indicate the field where the amplitude deviates from the standard form. In addition, it is clear from the changes that occur with the direction of H that there is significant variation of the carrier scattering time on this hole ellipsoid. The lines in the figure represent fits of the above form to the data carried out by varying the overall amplitude and Θ_D to find the best representation and these values are plotted in frame b of the figure. Here we observe a wide variation of Θ_D with the expected crystal symmetry including very large $\Theta_D \sim 20$ K near 20 and 63° from the [100]. In contrast, for $x = 0.05$ the field dependence of the dHvA amplitudes are all consistent with the standard form with Θ_D values scattered within $\sim 5^\circ$ of 25 K. In the inset to Fig. 6 we plot the x dependence of Θ_D determined for fields along the [100] direction for both measurement techniques. We observe a large increase in Θ_D for the V substituted samples as would be expected since the V impurities act as scattering centers for the charge carriers.

There are several possible reasons for deviations of the dHvA amplitude from the standard form, such as we observe at an angle of 30° in Fig. 6a, that we have considered. This includes magnetic breakdown, MB, and the effects of magnetic interaction. To explore the cause for the suppression of dHvA amplitudes with fields above 22 T, we plot in Fig. 7 the dHvA spectra for two orientations of the magnetic field taken over the field ranges noted in the figure. Each of these field ranges consists of equal intervals in $1/H$ corresponding to 20 oscillations of the λ orbital. The reproducibility of our data is apparent in the figure where we plot the spectra for both increasing and decreasing field for one of the orientations. These data reveal several interesting changes with magnetic fields near 22 T including a shift of spectral weight toward higher frequencies from 1450 T to 1625 T. In addition, oscillations with f of 700, and 2100 T and possibly at 150 T, although the field range in the figure corresponds to only 2 full oscillations at such a small frequency, become apparent only at higher fields. Such changes are indicative of magnetic breakdown orbits forming above ~ 22 T, which would account for our difficulties in determining Θ_D for these orientations. These changes are absent from our other samples on either side of the QCP sug-

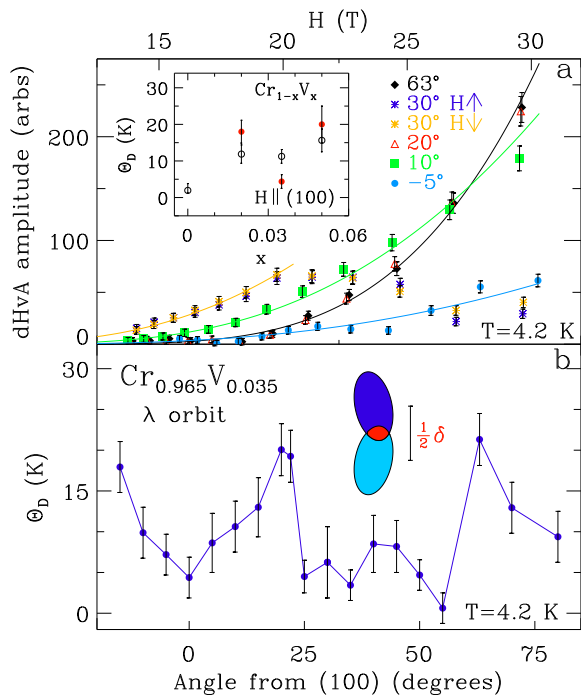


FIG. 6: (color online) Dingle Temperatures. a) Magnetic field, H , dependence of the amplitude of the torque cantilever de Haas-van Alphen signal for $x = 0.035$ associated with the N point (λ_1 orbit) of the bcc Brillouin zone at 4.2 K and several angles identified in the figure. Increments in $1/H$ containing 10 full oscillations of the dHvA signal were used to determine the amplitude plotted. A wide variation of the Dingle temperature, Θ_D , for different H orientations is apparent as well as a strong suppression at $H > 25$ T for H oriented 30° from the $[100]$ direction. Lines are fits to the standard form for determining Θ_D , see text[6]. Inset: V concentration, x , dependence of Θ_D for the λ orbit with H parallel to the $[100]$ direction for our pulsed field measurements, circles, and torque cantilever measurements, bullets. b) Angle dependence of Θ_D determined from our torque cantilever measurements. The angle refers to the orientation of H with respect to a $[100]$ crystal axis. Inset: Schematic representation of the N-pocket of the FS demonstrating the case where the remapping due to translation by the spin density wave vector causes minimal overlap.

gesting that it is a feature associated with samples with x just beyond x_c .

The accepted picture of $\text{Cr}_{1-x}\text{V}_x$ as x is varied includes the continuous modification of the FS as the charge carrier density is varied by the substitution. The result is a decreased ordered magnetic moment from the $0.4\mu_B$ of pure Cr, as well as a decreased wavevector for the SDW from $0.9513 a^*$ for pure Cr at 4 K down to 0.926 at $x = 0.025$ [31], and inelastic fluctuations at 0.92 for $x = 0.05$ [35]. The reduction of Q_{SDW} with x corresponds to an increased incommensurability which decreases the overlap of the N-pocket of holes with translation by nQ_{SDW} so that the overlap becomes zero near $x = 0.035$. For our sample nearest the critical concen-

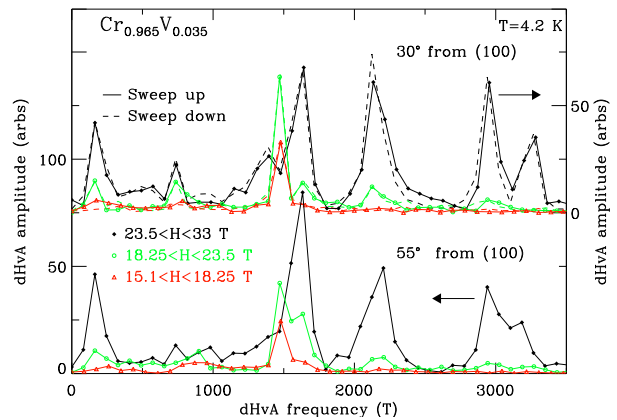


FIG. 7: (color online) de Haas-van Alphen spectrum over restricted field ranges. Torque cantilever dHvA spectra for a $\text{Cr}_{0.965}\text{V}_{0.035}$ crystal for field ranges identified in the figure for magnetic fields oriented 30° (top) and 55° (bottom) from a $[100]$. Field ranges were chosen so that equal ranges are $1/H$ are displayed.

tration, we observe magnetic breakdown in a restricted range of orientations of the magnetic field above 22 T for orbits that have long been associated with the N-pocket of holes. This contrasts with the magnetic breakdown orbits observed in nominally pure Cr, where a multitude of such frequencies is apparent even at the lowest fields (2 T) and in a wide range of directions[13–16]. In addition, our dHvA spectrum for $\text{Cr}_{0.98}\text{V}_{0.02}$ indicates such breakdown orbits at all fields where $\omega_c\tau > 1$ at all orientations that we probed. Associated with the magnetic breakdown at high field in $\text{Cr}_{0.965}\text{V}_{0.035}$ we find extraordinarily large Θ_D for magnetic field directions just outside of where the magnetic breakdown orbits are observed. We speculate that we may be witnessing a field induced SDW transition for magnetic fields above 22 T. The dependence on magnetic field direction suggests that the field modifies the Fermi surface in such a way as to enhance the nesting which lies at the root of the SDW phase in pure Cr. This is similar to the field induced SDW transition seen in the Bechgaard salt $(\text{TMTSF})_2\text{ClO}_4$ [36, 37] where magnetic fields modify the Fermi surface so that it is more one dimensional and, thus, more susceptible to the formation of a density wave phase. In the present case, while the magnetic field is not likely to reduce the effective dimensionality of the FS, we suggest that it modifies the FS in such a manner as to increase the areas which are nearly parallel and support nesting, but which do not change the FS volume. We note that the Landau level filling factor for the orbits observed is of order 50 in the field range where the MB is observed. This filling factor is sufficiently small so that subtle changes to the FS can be expected. However, these changes may be significant when in close proximity to the critical point. An example of a topological deformation of a Fermi surface has been observed in CeB_6 when subjected to strong mag-

netic fields[38]. Thus, field would tend to reverse the changes to the FS shape caused by V substitution and, perhaps, to mimic more closely the changes to Cr that occur with pressure[39]. This hypothesis may also explain the very large scattering rates indicated by the high Θ_D for field orientations just beyond where MB orbits are found. For these field directions the modification of the FS may only be sufficient to increase the SDW fluctuations leading to an enhanced scattering rate for carriers. Although this hypothesis is clearly speculative, our data are consistent with these ideas and experiments to search for a field induced SDW phase in $\text{Cr}_{0.965}\text{V}_{0.035}$ are suggested.

DISCUSSION AND CONCLUSIONS

Our exploration of the Fermi surface of $\text{Cr}_{1-x}\text{V}_x$ for V concentrations on both sides of the QCP at $x_c = 0.035$ employing dHvA oscillations has resulted in several important observations. The most conspicuous is the lack of dHvA oscillations associated with the large sheets of the FS thought to be responsible for the SDW formation in Cr for $x \geq x_c$. No dHvA signal from these FS sheets was observed despite the broad range of fields ($H \leq 55$ T for $x = 0.035$ and $H \leq 33$ T for $x = 0.05$) and orientations we have probed. This is in stark contrast to the observation of these same large FS sheets via dHvA in Mo and W at much lower fields as well as the observation of all of the Fermi surface sheets in Cr and $\text{Cr}_{1-x}\text{V}_x$ in ARPES and 2D-ACAR measurements that are less sensitive to carrier scattering. The absence of dHvA signals from FS sheets in $\text{Cr}_{1-x}\text{V}_x$ for $x \geq x_c$ other than the pocket of holes at the N-point, could be caused by a large scattering rate, a very large carrier effective mass, or a combination of both. Given that the electronic contribution to the specific heat, a Fermi surface average property, increases by less than a factor of 2 for $x \geq x_c$ [34] despite the factor of 2 increase in apparent carrier density[4, 5], we believe it unlikely that a large carrier mass is responsible. We are forced to conclude that the carriers on the larger FS sheets are more highly scattered than those associated with smaller hole FS sheet. The lack of dHvA oscillations allows us only to calculate a lower limit for the scattering rate of carriers residing on these sections of the FS, 2.5×10^{13} and $1.5 \times 10^{13} \text{ s}^{-1}$ for $x = 0.035$ and 0.05 respectively. These can be compared to estimates of the scattering rate made from transport measurements for carriers that reside on the FS sheets that survive the SDW formation of 4×10^{11} and $5 \times 10^{12} \text{ s}^{-1}$ for nominally pure and $x = 0.02$ single crystals respectively[4, 5].

It appears that although the electron jack and hole octahedron FS sheets, much celebrated because their nesting properties are responsible for SDW ordering, are likely restored for $x > x_c$, the strong SDW fluctuations create a large scattering rate for the carriers residing on

these FS sheets. This is consistent with inelastic neutron scattering experiments that indicate significant magnetic fluctuations even at V concentrations of $x = 0.05$ [35]. Thus, it follows that carrier scattering due to these fluctuations, or even the opening of a pseudogap derived from the antiferromagnetic fluctuations[4, 5], is responsible for the lack of dHvA signals from regions of the Fermi surface that are gapped in the SDW state.

Recent transport measurements on $\text{Cr}_{1-x}\text{V}_x$ have discovered a dramatic change in the Hall constant as x is increased through x_c , or equivalently pressure was increased through the critical pressure for the SDW AFM state[4, 5]. While the Hall effect in Cr, and $\text{Cr}_{1-x}\text{V}_x$ for $x < x_c$, demonstrates the opening of an energy gap over large fractions of the FS, for $x > x_c$ only the T -dependent effects of fluctuation scattering remain. Surprisingly, the changes in the resistivity are less dramatic[4, 5]. Models of the transport in $\text{Cr}_{1-x}\text{V}_x$ point out that the Hall conductivity is rather insensitive to the changes occurring on the flat regions of the Fermi surface, including those that are gapped as the SDW is formed[40, 41]. Instead, the changes to the Hall constant are shown to be due to variation of the longitudinal conductivity as the SDW phase is entered. Since the Hall constant is dependent on the square of the longitudinal conductivity, it is much more sensitive to the changes that occur at the SDW transition. Nonetheless, the relatively modest changes in the resistivity at T_N and at x_c that are observed, despite the gapping of a large fraction of the FS in the SDW state, can be understood if the carriers residing on the electron jack and hole octahedron are subject to significant fluctuation scattering in the paramagnetic state. The contribution to the longitudinal conductivity by these sections of FS is then small compared to that of FS sheets that are less involved in the SDW instability. Our data suggest that the pocket of holes centered at the N-point of the Brillouin zone experience a much smaller scattering rate and which may consequently dominate the carrier transport. This allows us to speculate that the non-Fermi liquid transport properties that are associated with magnetic QCPs in many materials may be absent in $\text{Cr}_{1-x}\text{V}_x$ simply because the scattering dependent electronic properties are dominated by FS sheets that are relatively unaffected by the SDW transition.

Our data show that hole ellipsoid centered on the N point of the Brillouin zone continues to dominate the dHvA spectra at $x > x_c$, demonstrate the existence of regions of large carrier scattering rates on this Fermi surface sheet, and hint at the possibility of a field induced SDW phase for x just beyond x_c . This last observation suggests a third possibility for probing the QCP in $\text{Cr}_{1-x}\text{V}_x$, application of large magnetic fields, which may be more straightforward than varying either the V concentration or the external pressure. Such an exploration may yield new physics and offer insight into the importance of time reversal invariance in determining the char-

acter of QCPs.

We are grateful to D. A. Browne and M. R. Norman for discussions. JFD acknowledges support from the National Science Foundation through DMR084376. A portion of this work was performed at the at the NHMFL, which is supported by National Science Foundation Cooperative Agreement No. DMR0654118, by the State of Florida, and by the Department of Energy.

* ditusa@phys.lsu.edu

- [1] C. G. Shull and M. K. Wilkinson *Rev. Mod. Phys.* **25**, 100 (1953).
- [2] See e.g. E. Fawcett, H.L. Alberts, V. Y. Galkin, D. R. Noakes, and J.V. Yakhmi, *Rev. Mod. Phys.* **66**, 25-127 (1994).
- [3] E. Fawcett, *Rev. Mod. Phys.* **60**, 209 (1988).
- [4] A. Yeh, Y-A. Soh, J. Brooke, G. Aeppli, T.F. Rosenbaum, and S.M. Hayden, *Nature* **419**, 459-462 (2002).
- [5] M. Lee, A. Husmann, T. F. Rosenbaum, and G. Aeppli, *Phys. Rev. Lett.* **92** 187201 (2004).
- [6] D. Shoenberg, *Magnetic Oscillations in Metals*, Cambridge University Press (Cambridge, 1984).
- [7] C. Capan, L. Balicas, T.P. Murphy, E.C.Palm, R. Movshovich, D. Hall, S. W. Tozer, M. F. Hundley, E. D. Bauer, J. D. Thompson, J. L. Sarrao, J. F. DiTusa, R. G. Goodrich, and Z. Fisk, *Phys. Rev. B* **80**, 094518 (2009).
- [8] S. K. Goh, J. Paglione, M. Sutherland, E. C. T. O'Farrell, C. Bergemann, T. A. Sayles, and M. B. Maple, *Phys. Rev. Lett.* **101**, 056402 (2008).
- [9] C. Jaudet, D. Vignolles, A. Audouard, J. Levallois, D. LeBoeuf, N. Doiron-Leyraud, B. Vignolle, M. Nardone, A. Zitouni, R. Liang, D. A. Bonn, W. N. Hardy, L. Taillefer, and C. Proust, *Phys. Rev. Lett.* **100**, 187005 (2008).
- [10] R. Settai, H. Shishido, T. Kubo, S. Araki, T. C. Kobayashi, H. Harima, and Y. Onuki, *J. Mag. Mag. Mat.* **310**, 541-547 (2007).
- [11] R. G. Goodrich, N. Harrison, and Z. Fisk, *Phys. Rev. Lett.* **97**, 146404 (2006).
- [12] P. M. C. Rourke, A. McCollam, G. Lapertot, G. Knebel, J. Flouquet, and S. R. Julian, *Phys. Rev. Lett.* **101**, 237205 (2008).
- [13] J. E. Graebner and J. A. Marcus, *Phys. Rev.* **175**, 659 (1968).
- [14] E. Fawcett, R. Griessen, and D. J. Stanley, *J. Low Temp. Phys.* **25**, 771 (1976).
- [15] W. J. Venema, R. Griessen, and W. Ruesink, *J. Phys. F* **10**, 2841-2856 (1980).
- [16] D. W. Ruesink and I. M. Templeton, *J. Phys. F* **14**, 2395-2409 (1984).
- [17] Y. Tsunoda, M. Mori, N. Kunitomi, Y. Teraoka, and J. Kanamori, *Solid State Commun.* **14**, 287 (1974).
- [18] W. M. Lomer, *Proc. Phys. Soc.* **80** 489-496 (1962).
- [19] J. L. Fry, N. E. Brener, D. G. Laurent, and J. Callaway, *J. Appl. Phys.* **52**, 2101 (1981).
- [20] L. F. Mattheiss, *Phys. Rev.* **139**, A1893-A1904 (1965).
- [21] G. deVreis, *J. Phys. Rad.* **20**, 438-439 (1959).
- [22] A. L. Trego and A. R. Mackintosh, *Phys. Rev.* **166**, 495 (1968).
- [23] A. J. Arko, J. A. Marcus, and W. A. Reed, *Phys. Rev.* **176**, 671 (1968).
- [24] R. Reifenberger, F. W. Holroyd, and E. W. Fawcett, *J. Low Temp. Phys.* **38**, 421 (1980).
- [25] J.A. Hoekstra and J. L. Stanford, *Phys. Rev. B* **8** 1416 (1973).
- [26] R. F. Girvan, A. V. Gold, and R. A. Phillips, *J. Phys. chem. Solids* **29**, 1485 (1968).
- [27] O. Krupin, E. Rotenberg, and S. D. Kevan, *Phys. Rev. Lett.* **99**, 147208 (2007).
- [28] J. Schafer, E. Rotenberg, G. Meigs, S.D. Kevan, P. Blaha, and S. Hufner, *Phys. Rev. Lett.* **83**, 2069 (1999).
- [29] R. J. Hughes, S. B. Dugdale, Zs. Major, M. A. Alam, T. Jarlborg, E. Bruno, and B. Ginatempo, *Phys. Rev. B* **69**, 174406 (2004).
- [30] A. J. Gutman and J. L. Stanford, *Phys. Rev. B* **4**, 4026 (1971).
- [31] W. C. Koehler, R. M. Moon, A. L. Trego, and A. R. Mackintosh, *Phys. Rev.* **151**, 405 (1966).
- [32] S. Araj, *Can. J. Phys.* **47**, 1005 (1969).
- [33] R. G. Goodrich, N. Harrison, J. J. Vuillemin, A. Teklu, D. W. Hall, Z. Fisk, D. Young, and J. Sarrao, *Phys. Rev. B* **58**, 14896 (1998).
- [34] F. Heiniger, *Phys. Kondens. Mater.* **5**, 285 (1966).
- [35] S. M. Hayden, R. Doubble, G. Aeppli, T. G. Perring, and E. Fawcett, *Phys. Rev. Lett.* **84**, 999 (2000).
- [36] F. Pesty, P. Garoche, and K. Bechgaard, *Phys. Rev. Lett.* **55**, 2495 (1985).
- [37] P. M. Chaikin, E. I. Chashechkina, I. J. Lee, and M. J. Naughton, *J. Phys. Cond. Mat.* **10**, 11301-11314 (1998).
- [38] N. Harrison, D. W. Hall, R. G. Goodrich, J. J. Vuillemin, and Z. Fisk, *Phys. Rev. Lett.* **81**, 870 (1998).
- [39] Y. Feng, R. Jaramillo, G. Srajer, J.C. Lang, Z. Islam, M. S. Somayazulu, O.G. Shpyrko, J.J. Pluth, H.-k. Mao, E.D. Isaacs, G. Aeppli, and T.F. Rosenbaum, *Phys. Rev. Lett.* **99**, 137201 (2007).
- [40] M.R. Norman, Q. Si, Ya. B. Bazaliy, and R. Ramazashvili, *Phys. Rev. Lett.* **90**, 116601 (2003).
- [41] Ya. B. Bazaliy, R. Ramazashvili, Q. Si, and M. R. Norman, *Phys. Rev. B* **69**, 144423 (2004).